Human Molecular Genetics, 2002, Vol. 11, No. 5 525–534

A mouse model of TSC1 reveals sex-dependent lethality from liver hemangiomas, and up-regulation of p70S6 kinase activity in Tsc1 null cells

David J. Kwiatkowski*, Hongbing Zhang, Jennifer L. Bandura, Kristina M. Heiberger, Michael Glogauer, Nisreen el-Hashemite and Hiroaki Onda

Genetics Laboratory, Hematology Division, Brigham and Women's Hospital, Harvard Medical School, 221 Longwood Avenue, LM-302, Boston, MA 02115, USA

Received October 26, 2001; Revised and Accepted December 30, 2001

Tuberous sclerosis (TSC) is a autosomal dominant genetic disorder caused by mutations in either TSC1 or TSC2, and characterized by benign hamartoma growth. We developed a murine model of Tsc1 disease by gene targeting. Tsc1 null embryos die at mid-gestation from a failure of liver development. Tsc1 heterozygotes develop kidney cystadenomas and liver hemangiomas at high frequency, but the incidence of kidney tumors is somewhat lower than in Tsc2 heterozygote mice. Liver hemangiomas were more common, more severe and caused higher mortality in female than in male Tsc1 heterozygotes. Tsc1 null embryo fibroblast lines have persistent phosphorylation of the p70S6K (S6K) and its substrate S6, that is sensitive to treatment with rapamycin, indicating constitutive activation of the mTOR-S6K pathway due to loss of the Tsc1 protein, hamartin. Hyperphosphorylation of S6 is also seen in kidney tumors in the heterozygote mice, suggesting that inhibition of this pathway may have benefit in control of TSC hamartomas.

INTRODUCTION

Tuberous sclerosis (TSC) is an autosomal dominant tumor suppressor gene syndrome, characterized by development of distinctive benign tumors (hamartomas) and malformations (hamartias) in multiple organ systems (1). The brain, skin, heart and kidneys are commonly affected. Less commonly, female TSC patients develop pulmonary lymphangioleiomyomatosis (LAM) (1–3). TSC hamartomas are often composed of multiple cell types, including smooth muscle cells, perivascular epithelioid cells, endothelial cells, adipocytes and large neuronal appearing cells. Despite this diversity of cell types, most lesions in TSC appear to be clonal in nature, based upon clonality and LOH analyses (4–8), fitting with a two-hit model for pathogenesis.

Two genes have been identified that cause TSC: TSC1 on 9q34 encoding the protein hamartin, and TSC2 on 16p13 encoding the protein tuberin (9,10). Tuberin may have functions as a GTPase activating protein for the small GTPases rap1 and/or rab5 (11,12) and also appears to be involved in cell-cycle control and transcriptional events (13–15). Hamartin may function in adhesion events and in rho-dependent signalling for actin stress fibre formation (16). The two proteins occur in a stable complex, suggesting that their function is interdependent (17,18).

TSC is transmitted in an autosomal dominant fashion, though most cases are sporadic representing new mutational events (1,19). The great majority of mutations in these genes are clearly inactivating (20–22). The disease varies greatly in its severity, and although there is significant overlap, mutations in TSC1 cause clinical features that are somewhat milder than mutations in TSC2 (22).

Both rat and mouse models of TSC2 disease have been identified or generated (23–27). These models have similar features, with prominent development of multiple renal cystadenomas that progress slowly to malignancy over the lifetime of the rodent. Several other tumors are also seen, with liver hemangiomas seen in the mouse models.

Recent studies in *Drosophila* have implicated a defect in cell size regulation in dTsc1 or dTsc2 null cells and a possible relationship of these genes to the PI3kinase-Akt/PKB-S6K signalling pathway (28–30).

RESULTS

Generation of mice with a targeted, disrupted Tsc1 allele

To assess the function of Tsc1 in the mouse, a Tsc1 null mutation was generated in a two-step gene targeting procedure using embryonal stem (ES) cells (Fig. 1A). Southern blot analysis indicated successful gene targeting (Fig. 1B), which was followed by cre recombinase expression to yield an allele of Tsc1 in which exons 17 and 18 are deleted (Fig. 1C). Blastocyst injection led to germline transmission of the mutant Tsc1 allele as confirmed by Southern blot (data not shown) and PCR genotyping

*To whom correspondence should be addressed. Tel: +1 617 278 0384; Fax: +1 617 734 2248; Email: dk@rics.bwh.harvard.edu

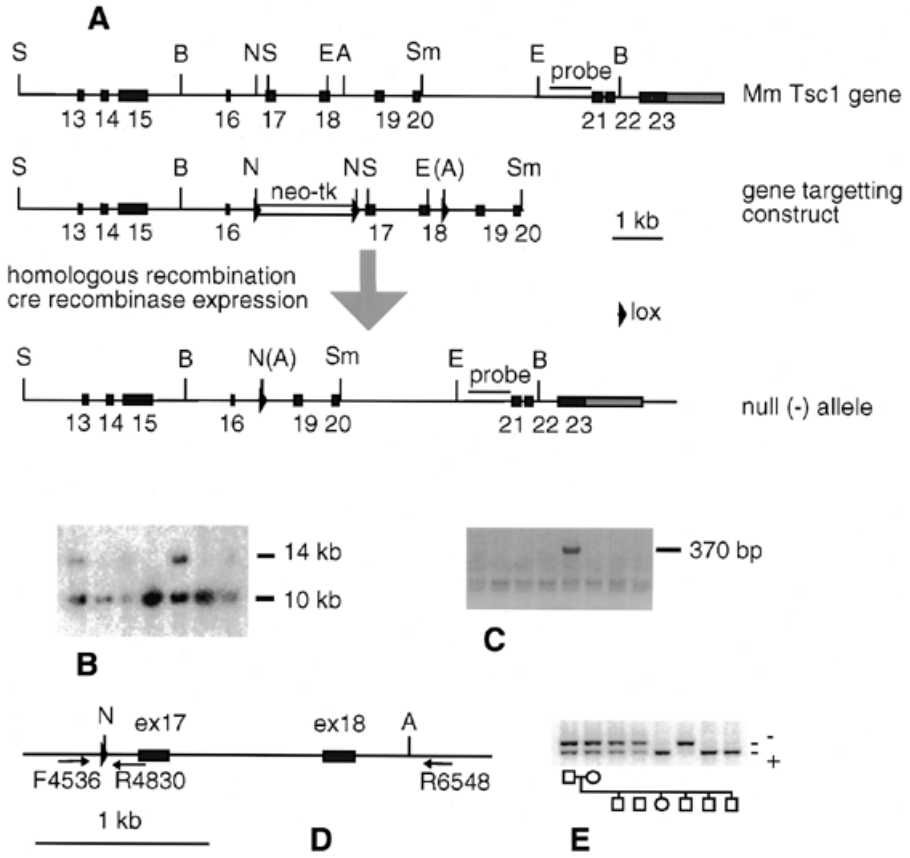

Figure 1. Generation of mice with a targeted, disrupted Tsc1 allele. (**A**) Genomic structure of the Tsc1 gene, the Tsc1 targeting construct, and the structure of the null, Tsc1^{-} allele. A, *Avr*II; B, *Bsa*BI; E, *Eco*RI; N, *Nhe*I; S, *Sac*I; Sm, *Sma*I. (**B**) Southern blot analysis of *Bsa*BI-digested ES cell DNA demonstrating an enlarged band due to insertion of the neo-TK cassette into the Tsc1 gene in two of seven clones. (**C**) PCR analysis demonstrating deletion of exons 17 and 18 in one of eight ES cell subclones, isolated after cre expression. Primers used were F4536 and R6548. (**D**) Diagram of the primers used to genotype the wild-type and null Tsc1 alleles. (**E**) PCR genotyping of Tsc1$^{+/-}$ parents and their litter of E11 embryos. One null embryo is identified in this litter.

analyses (Fig. 1D and E). Deletion of exons 17 and 18 from Tsc1 results in termination of translation as the message goes out of reading frame, and is similar to mutations naturally occurring in Tsc1 (21) (http://expmed.bwh.harvard.edu/ts/review/). In addition, immunoblot analyses (see below) indicated that there was no hamartin produced from this allele, so we refer to it as Tsc1^{-}.

Homozygous Tsc1$^{-/-}$ is embryonic lethal

Homozygous Tsc1$^{-/-}$ mice were not obtained from Tsc1$^{+/-}$ intercrosses, indicating that this Tsc1^{-} allele had a recessive lethal phenotype (Table 1). To explore the timing of embryonic death, embryos were obtained from Tsc1$^{+/-}$ × Tsc1$^{+/-}$ breedings at embryonic day 9 (E9)–E14.5. No viable Tsc1$^{-/-}$ embryos were observed beyond E13.5. At E9–13.5, considering both viable and partially resorbed embryos, Tsc1$^{-/-}$ embryos were present in the expected Mendelian ratio. However, viability of embryos steadily declined from E9–9.5 to E13–13.5. Survival of Tsc1$^{-/-}$ embryos was significantly improved over that of Tsc2 null embryos (27). None of 50 E13–13.5 Tsc2$^{+/-}$ intercross embryos were Tsc2$^{-/-}$ in comparison with seven (two viable) of 32 Tsc1$^{+/-}$ intercross embryos which were Tsc1$^{-/-}$ as shown here ($P = 0.0005$).

Viable E9–12.5 Tsc1$^{-/-}$ embryos were less developed to a variable extent, typically by approximately one embryonic day, in comparison with Tsc1$^{+/+}$ and Tsc1$^{+/-}$ littermates, but no exencephaly was seen among the 33 viable null embryos examined or among their non-viable null littermates (Fig. 2A and D). Tsc1$^{-/-}$ embryos were also paler and edematous, and often had pericardial effusions. Histologic analysis of viable Tsc1$^{-/-}$ E9–11.5 embryos demonstrated a hypoplastic liver with poor development of other abdominal organs, and a slightly enlarged heart that was shifted inferiorly (Fig. 2B and E). The liver and other abdominal organs had dilated vascular channels (Fig. 2C and F). Embryonic death appeared to be due to liver hypoplasia with secondary growth retardation and circulatory failure from anemia. Brain development, as assessed by neuroepithelial cell proliferation and organization (Fig. 2B and E), was mildly retarded in the Tsc1$^{-/-}$ embryos, consistent with their overall developmental delay. These results are similar to those seen for the null allele of Tsc2 (27), although exencephaly was seen in some Tsc2$^{-/-}$ embryos.

Survival of female Tsc1$^{+/-}$ mice is reduced due to hepatic hemangiomas

Defined cohorts of F1 generation mice were tracked for survival from birth until 15–18 months of age. The cohorts

Table 1. Viability of Tsc1$^{+/-}$ intercross embryos according to age

Embryonic day	Number of embryos with genotype:			Percent –/– embryos		Number of embryos	
	+/+	+/–	–/–	Total	Viable	Genotyped	Resorbed[a]
28 pp	104	195	0	0		NA	
E14–14.5	10	18	0 (5)	15%	0%	33	6
E13–13.5	9	15 (1)	2 (5)	22%	8%	32	3
E12–12.5	6 (1)	18 (1)	3 (4)	21%	11%	33	0
E11–11.5	28	37 (3)	13 (8)	24%	17%	89	6
E10–10.5	14 (3)	29 (2)	13 (5)	27%	23%	66	4
E9–9.5	3	4	2	22%	22%	9	0

Numbers in parentheses refer to resorbing embryos that could be genotyped. pp, post-partum.
[a]Indicates resorption sites from which no material could be obtained for genotyping.

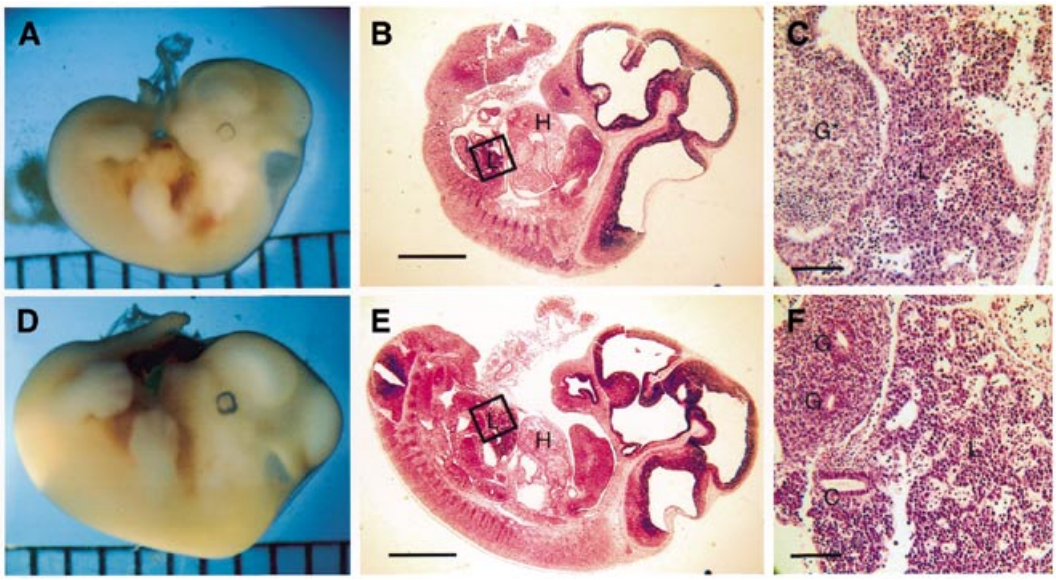

Figure 2. Analysis of Tsc1$^{-/-}$ embryos. Gross anatomy and histology of Tsc1$^{-/-}$ (**A–C**) and wild-type (**D–F**) embryos at E11.5. (A and D) External view, 1 mm ruler in background. (B and E) Full embryo sagittal section. Box indicates area of view enlarged in (C and F). H, heart; L, liver. Note small size of Tsc1 null liver, which was seen on only a few serial sections. Also note that the neuroepithelial cell layer, lining the ventricles, appears somewhat larger in the wild-type embryo. (C and F) Liver and adjacent organs. G, gut; L, liver; C, gallbladder. Note the dilated vascular channels in the null liver and absence of early enteric channels in the Tsc1 null gut (G*). Bars are 1 mm (B and E) and 0.1 mm (C and F).

consisted of 10 wild-type mice (five female, five male) and 20 each of male and female Tsc1$^{+/-}$ mice (Tables 2–4). Ten percent (one of 10, a male) of control and 10% (two of 20) of male Tsc1$^{+/-}$ mice died prior to 18 months of age. In contrast, 45% (nine of 20) of female Tsc1$^{+/-}$ mice died (including one mouse killed for humane reasons) prior to 18 months of age (Fig. 3A; $P = 0.015$ in comparison with male Tsc1$^{+/-}$). Necropsy exam could not be performed on four females who died due to autolysis or cannibalism by cagemates. Three of the four female mice who died prematurely showed a large amount of blood in the peritoneal cavity which appeared to be derived from a vascular tumor in the liver. Five female and two male F1 mice were pure 129/SvJae strain, of which five died prematurely, and two of these had necropsy exams showing blood in the peritoneal cavity. The Tsc1$^{+/-}$ genotype therefore appeared to cause more severe liver disease in a pure 129SvJae background. The survival analysis was repeated using only the hybrid strain mice, and Tsc1$^{+/-}$ females again showed a reduction in survival compared to Tsc1$^{+/-}$ males (data not shown, $P = 0.05$).

Table 2. Pathologic findings in aged cohorts of F1 Tsc1$^{+/-}$ mice (15–18 months): cohort definition, strains and premature mortality

Cohort	Strains[a]				
	Total	B	C	129	Premature death
Wild-type	10	4	6	0	1
Tsc1$^{+/-}$ males	20	4	14	2	2
Tsc1$^{+/-}$ females	20	8	7	5	9[b]

[a]Strains of these F1 mice are: B, BALB/c-129/SvJae hybrid; C, C57BL/6-129/SvJae hybrid; 129, 129/SvJae.
[b]This includes one mouse killed for humane reasons.

Histologic analysis demonstrated that the vascular hepatic lesions were hemangiomas, consisting of aberrant vascular

Table 3. Pathologic findings in aged cohorts of F1 $Tsc1^{+/-}$ mice (15–18 months): severity of kidney and liver tumors

Genotype, strain	*n*	Kidney[a]				Liver[b]			
		<1	1–1.5	1.5–2	>2	0	1	2	3
Wild-type	10	0.1	0	0	0	10	0	0	0
$Tsc1^{+/-}$ B males	4	9	2.7	1.2	0.5	1	1	2	0
$Tsc1^{+/-}$ C males	13	4.1	2.2	0.3	0.2	5	0	7	1
$Tsc1^{+/-}$ 129 males	1	3	1	0	0	0	0	0	1
All $Tsc1^{+/-}$ males	18	5.1	2.2	0.5	0.3	6	1	9	2
$Tsc1^{+/-}$ B females	7	12.7	3.4	0.7	0.6	1	0	3	3
$Tsc1^{+/-}$ C females	5	3.4	1.8	0.4	0.2	0	0	2	3
$Tsc1^{+/-}$ 129 females	1	4	0	0	0	0	0	0	1
All $Tsc1^{+/-}$ females	13	8.5	2.5	0.5	0.4	1	0	5	7

[a]Average number of kidney lesions per mouse, grouped according to size in mm, as determined by external inspection.
[b]Number of mice with liver lesions graded as: 0, not present; 1, microscopic; 2, grossly visible but localized; 3, multilobar.

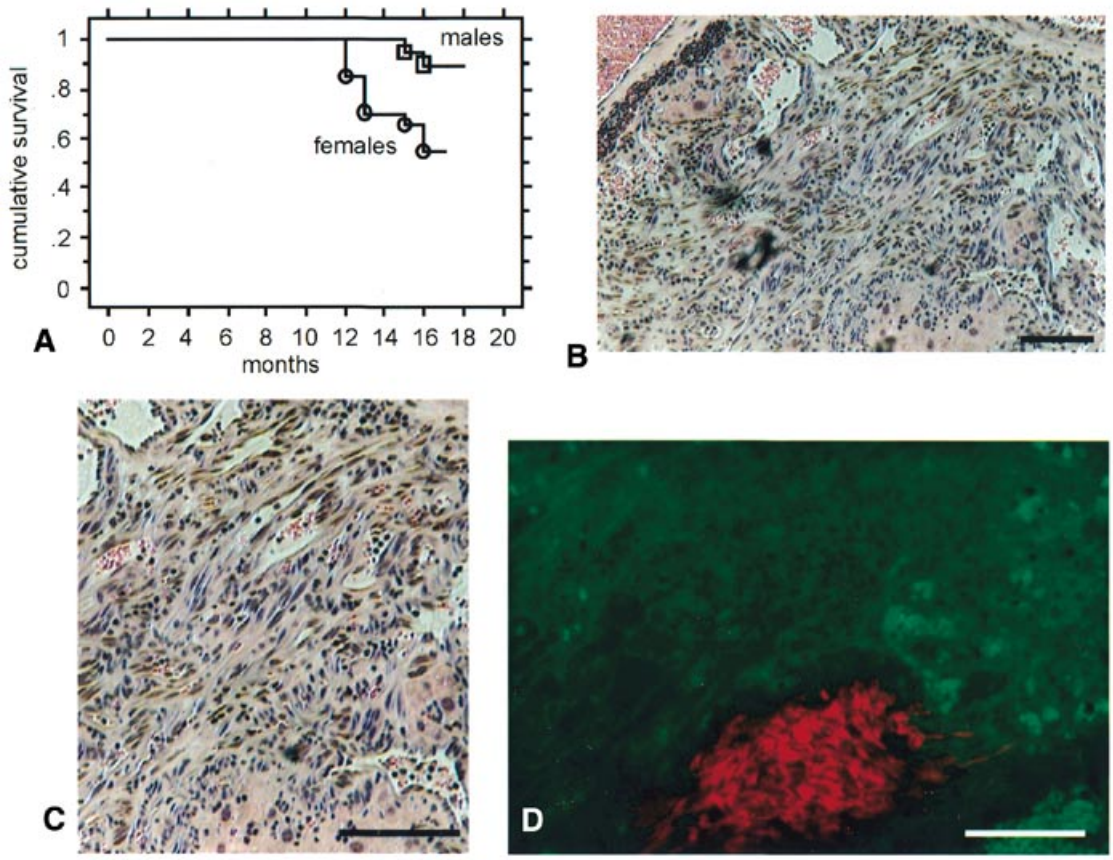

Figure 3. Survival and liver hemangiomas in $Tsc1^{+/-}$ mice. (**A**) Kaplan–Meier cumulative survival plot for male and female F1 $Tsc1^{+/-}$ mice. (**B** and **C**) Liver hemangioma. In (B) the structure at upper left is a small portion of a large aberrant vascular channel. Note the disorganized stroma with smooth muscle cells and many small vascular spaces. (**D**) Smooth muscle cells in a hemangioma. The red color is due to the Cy3 signal on the anti-smooth muscle actin antibody; green is liver autofluorescence. Bars are 100 μm.

channels of highly variable size that often had cuboidal–columnar endothelial cells, and proliferation of smooth muscle cells (Fig. 3B and C). This cellular identification was confirmed by immunohistochemical staining for smooth muscle actin (Fig. 3D). Among $Tsc1^{+/-}$ mice surviving to 15–18 months of age, these lesions were seen in 67% males and 93% females (Table 4). These lesions also had a higher average grade in female compared to male $Tsc1^{+/-}$ mice ($P = 0.03$, Fisher's exact test).

Table 4. Pathologic findings in aged cohorts of F1 Tsc1$^{+/-}$ mice (15–18 months): fraction of mice with tumors

Genotype, strain	*n*	Kidney cystadenoma	carcinoma	Lung adenoma	Liver hemangioma	Extremity angiosarcoma
Wild-type	10	1 (10%)	0	4 (40%)	0	0
Tsc1$^{+/-}$ B males	4	4 (100%)	1 (25%)	1 (25%)	3 (75%)	1 (25%)
Tsc1$^{+/-}$ C males	13	13 (100%)	4 (31%)	3 (23%)	8 (62%)	0
Tsc1$^{+/-}$ 129 males	1	1 (100%)	0	1 (100%)	1 (100%)	0
All Tsc1$^{+/-}$ males	18	18 (100%)	5 (28%)	5 (28%)	12 (67%)	1 (6%)
Tsc1$^{+/-}$ B females	7	7 (100%)	0	2 (29%)	6 (86%)	0
Tsc1$^{+/-}$ C females	5	5 (100%)	1 (20%)	2 (40%)	5 (100%)	0
Tsc1$^{+/-}$ 129 females	1	1 (100%)	0	0	1 (100%)	0
All Tsc1$^{+/-}$ females	13	13 (100%)	1 (8%)	4 (31%)	12 (92%)	0

Thus, these lesions were more frequent, of larger size and caused death more commonly in female compared to male Tsc1$^{+/-}$ mice, independent of strain.

Other tumors in the Tsc1$^{+/-}$ mice

Multiple bilateral renal cystadenomas developed in all Tsc1$^{+/-}$ mice by 15–18 months of age. The histologic features of these tumors were similar to those seen in Tsc2$^{+/-}$ mice (27) and varied from pure cysts with cuboidal lining cells to cysts with papillary projections, to solid adenomas (Fig. 4A). These lesions expressed gelsolin (Fig. 4B), similarly to Tsc2$^{+/-}$ mouse cystadenomas (27) and consistent with the renal intercalated cell as the cell of origin. A small fraction (Table 4) of these tumors showed histologic features consistent with progression to renal cell carcinoma (Fig. 4C and D), but there was no evidence of metastasis. In contrast to the findings with liver hemangiomas, there was no difference in the number or size of kidney cystadenomas according to sex. However, there were more cystadenomas in BALB/c-129/Sv hybrid mice (mean number adjusted for sex and age 16.03) in comparison to either the C57/BL6-129/Sv hybrid (adjusted mean 6.56, $P < 0.05$) or the 129/Sv mice (adjusted mean 4.28, $P < 0.05$) (Table 2).

A single male mouse developed a hemangiosarcoma of the forepaw. Lung adenomas were seen at approximately equal frequency in Tsc1$^{+/-}$ and control mice, suggesting that its pathogenesis was independent of the Tsc1 gene.

To rigorously assess the possibility of a difference in the severity of renal cystadenomas in Tsc1$^{+/-}$ compared to Tsc2$^{+/-}$ mice (27), a blinded comparison was made using microscopic sections from the kidneys of F1 mice for each gene (Table 5). Tsc2$^{+/-}$ mice had significantly more cysts than Tsc1$^{+/-}$ mice in an overall comparison adjusted for strain and sex ($P = 0.0004$). However, in a similar adjusted comparison, there was no significant difference in the number or size of adenomas in the Tsc2$^{+/-}$ and Tsc1$^{+/-}$ mice.

Analysis of Tsc1 null fibroblasts

To derive cells in which the function of hamartin, the Tsc1 gene product, could be examined, we cultured murine embryo fibroblasts (MEFs) from E10.5 embryos of Tsc1$^{+/-}$ intercrosses. MEF cultures were readily established, but Tsc1 null MEFs displayed a slower growth rate within several passages,

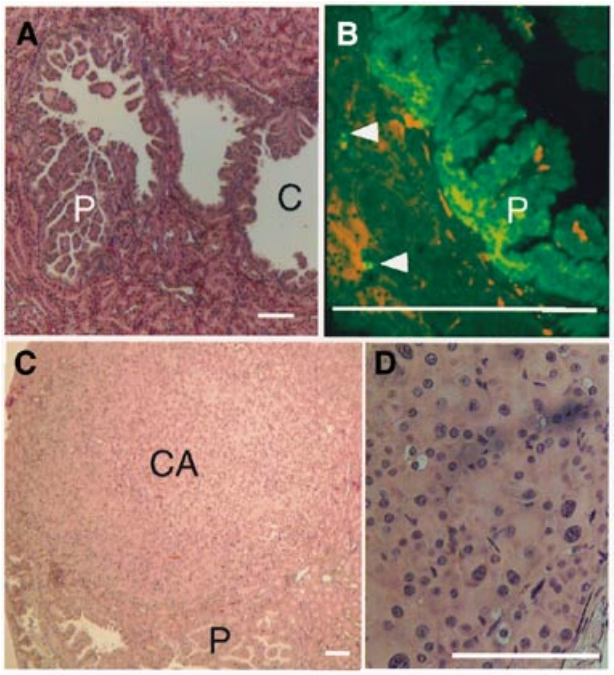

Figure 4. Pathology of kidney tumors in Tsc1$^{+/-}$ mice. (**A**) Complex cystadenoma is seen with regions that appear more cyst-like (right, C) and regions that have more papillary growth (left, P). (**B**) Gelsolin expression by a cystadenoma. Gelsolin (light green signal) is expressed strongly by the papillary tumor (P) while single intercalated cells (white arrowheads) also express gelsolin. (**C**) Kidney carcinoma (CA) which appears to have developed from an adjacent papillary cystadenoma (P) (**D**) Kidney carcinoma, high power view, demonstrating nuclear pleomorphism. Bars are 100 μm.

in comparison with Tsc1$^{+/-}$ or wild-type MEFs (Fig. 5A). Spontaneously immortalized cell lines were obtained from three Tsc1$^{+/+}$ and three Tsc1$^{+/-}$ MEF cultures, and from two of three Tsc1$^{-/-}$ cultures. These cell lines displayed variability in growth rates that did not correlate with genotype, consistent with stochastic clonal variation (doubling times for four lines were: Tsc1$^{-/-}$, 0.53 days; Tsc1$^{-/-}$, 2.32 days; Tsc1$^{+/+}$, 2.06 days; Tsc1$^{+/-}$, 0.61 days).

We examined the actin cytoskeleton and focal adhesion content in two Tsc1$^{+/+}$ and two Tsc1$^{-/-}$ cell lines. All four lines

Table 5. Comparison of renal cyst and adenoma development in $Tsc1^{+/-}$ versus $Tsc2^{+/-}$ mice

	$Tsc1^{+/-}$	$Tsc2^{+/-}$	*P*-value
n	22	16	
Cysts	2.55	8.01	0.0004
Adenomas	10.76	12.05	0.4510
Size of adenomas (mm)	0.75	0.78	0.5209

Mean number of cysts and adenomas, as well as mean size of adenomas, adjusted for background and sex, are shown. Cysts and adenomas were identified by blinded reading of five H&E sections per kidney. For this analysis, cysts with papillary projections were counted as cysts if less than half the cyst was filled; otherwise they were counted as adenomas.

demonstrated an increase in F-actin content (assessed by phalloidin staining) and focal adhesion formation (assessed by paxillin staining) in response to serum stimulation after overnight serum starvation. However, there was a significantly smaller increase ($P < 0.05$) in both F-actin levels and paxillin staining in the Tsc1 null lines compared to the wild-type lines (Fig. 5B and C).

Analysis of the PI3kinase-Akt/PKB-mTOR-S6K pathway

We also examined the expression and activation of the PI3kinase-Akt/PKB-mTOR-S6K signalling pathway in these cell lines. During serum deprivation followed by serum stimulation, clear differences between Tsc1 null and wild-type or $Tsc1^{+/-}$ cell lines were seen (Fig. 6A). As expected, hamartin could not be detected in Tsc1 null lines, confirming that this was a null allele. Levels of ERK and p-ERK were similar in both sets of lines, although p-ERK levels were somewhat reduced after serum stimulation in the Tsc1 null cells. More strikingly, Akt failed to undergo phosphorylation in Tsc1 null cells after serum stimulation. In addition, although levels of S6K were similar in both sets of cells, there was constitutive phosphorylation of S6K in the Tsc1 null cells during serum starvation.

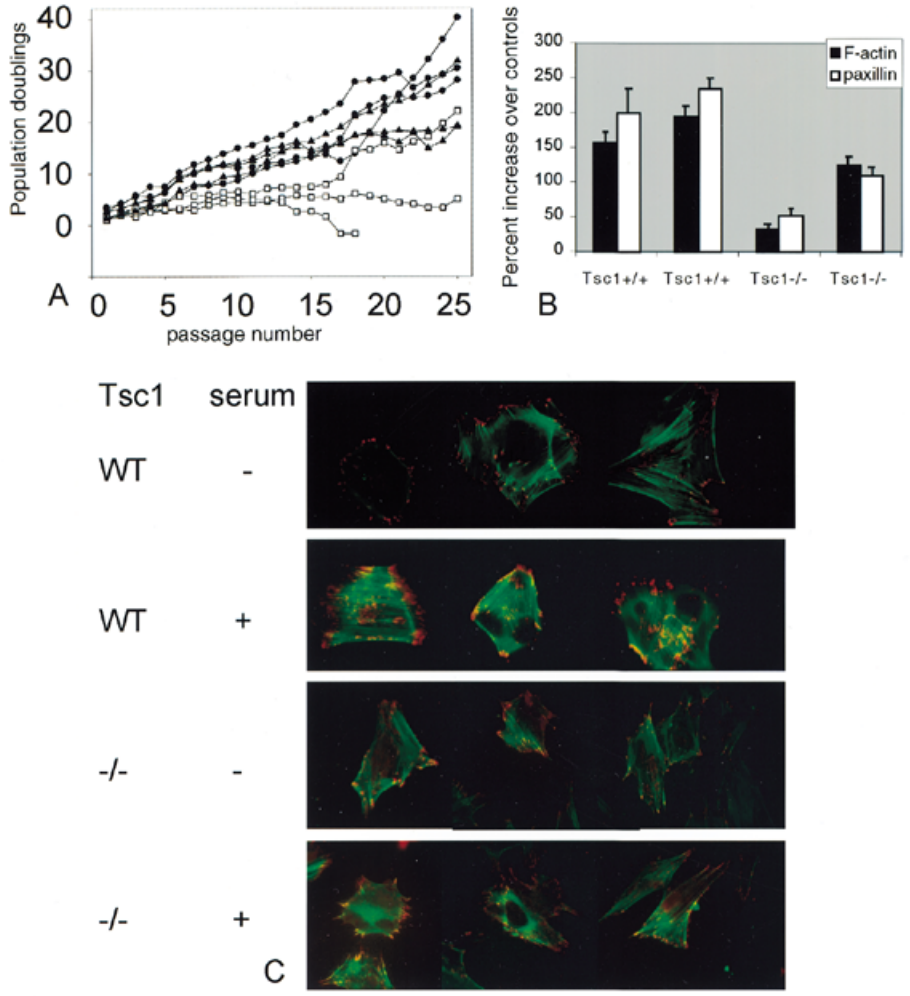

Figure 5. Growth and actin dynamics in Tsc1 null MEFs. (**A**) Growth curve indicating the population doublings (*y*-axis) in $Tsc1^{+/-}$ intercross-derived MEF cultures, according to passage number (*x*-axis). Solid circles, $Tsc1^{+/+}$; solid triangles, $Tsc1^{+/-}$; open squares, $Tsc1^{-/-}$. (**B**) Actin and focal adhesion dynamics. The percent increase in F-actin and focal adhesions, as assessed by rhodamine–phalloidin and paxillin staining, in cells following 24 h serum deprivation and 1 h of serum restimulation. Larger increases in F-actin and focal adhesions are seen in the wild-type in comparison to Tsc1 null lines ($P < 0.05$). (**C**) Representative fields of actin and focal adhesion staining. Note the greater increase in both F-actin and paxillin staining after serum addition, in comparison to relatively little change in the Tsc1 null cells.

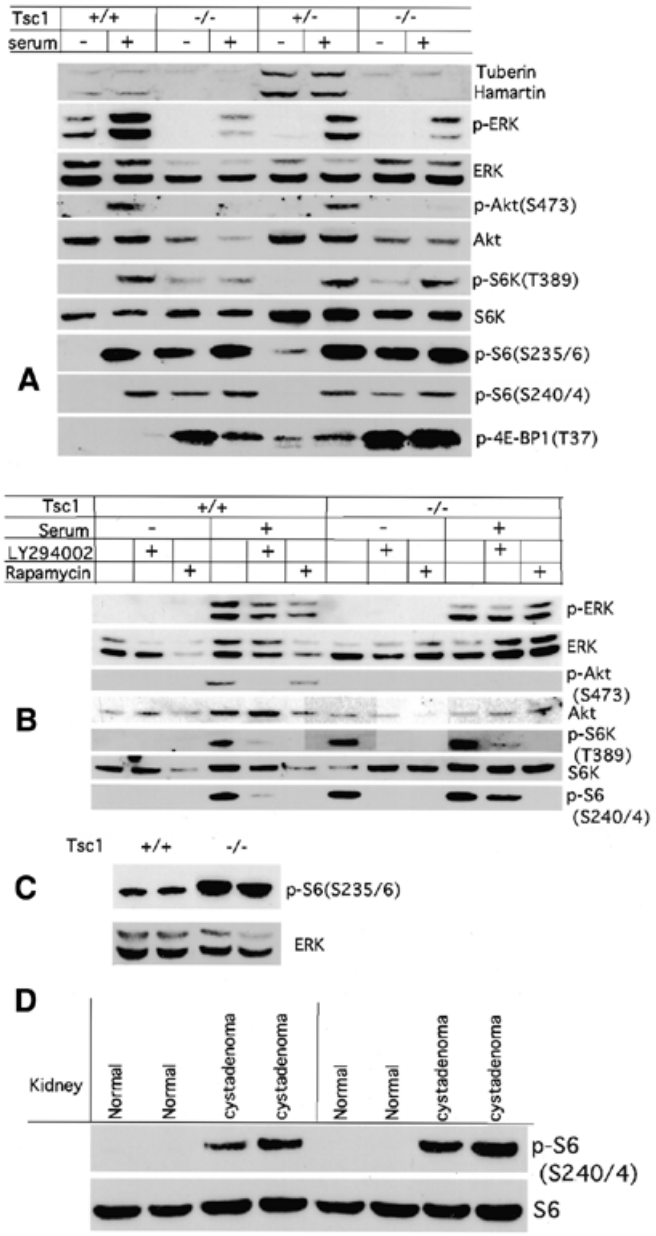

Figure 6. Deregulation of Akt-S6K signalling in Tsc1 null cells. (**A**) Expression and phosphorylation of ERK, Akt, S6K, S6 and 4E-BP1 in wild-type and Tsc1 null cells following 2 days serum deprivation, with or without 1 h serum restimulation. Expression of tuberin and hamartin is also shown. Four different cell lines analyzed. p-S6K, p-S6 and p-4E-BP1 levels are increased without serum stimulation in the null cell lines. (**B**) Expression and phosphorylation of these proteins after 24 h serum starvation, and combinations of 1 h pre-treatment with LY294002 (10 μM) or rapamycin (10 nM), and 1 h treatment with 10% serum. pS6K and pS6 levels in the Tsc1 null cells are reduced by treatment with rapamycin. (**C**) Expression of phosphorylated S6 and ERK in P4 MEFs, two $Tsc1^{-/-}$ and two wild-type lines. (**D**) Expression and phosphorylation of S6 in normal kidney and cystadenomas from two $Tsc1^{+/-}$ mice.

Moreover, the ribosomal protein S6, a target of S6K whose translational activity is activated by phosphorylation, was constitutively phosphorylated in the null cells. In addition, levels of p-S6K and p-S6 were not increased further with serum stimulation in the Tsc1 null cells. Levels of phosphorylated 4E-BP1 were also increased in the Tsc1 null cells during serum starvation.

We then investigated the response of these cell lines to the PI3K inhibitor LY294002 and the mTOR inhibitor rapamycin (Fig. 6B). Phosphorylation of both S6K and S6 was eliminated in serum-starved Tsc1 null cells by treatment with either LY294002 or rapamycin. With serum stimulation, however, rapamycin treatment was more effective in eliminating phosphorylation of these proteins.

To be certain that the observed differences were not due to changes associated with immortalization of these MEF cultures, we also assayed ERK, pS6K and pS6 levels in extracts prepared from passage four (P4) primary cultures of Tsc1 null and wild-type MEFs. pS6K could not be identified in these assays, probably due to cell number and/or antibody limitations. However, levels of pS6 were clearly increased in the Tsc1 null P4 MEFs compared to wild-type (Fig. 6C), implicating increased S6K activity in these cells.

We then investigated expression of S6K, p-S6K, S6 and p-S6 in tumors derived from the Tsc1 heterozygote mice (Fig. 6D). Levels of S6 were the same in adjacent normal kidney tissue and cystadenomas. In contrast, levels of p-S6 were increased substantially in all cystadenomas. p-S6K could not be identified in extracts from these tumors, but this may be due to contamination by normal cells or antibody limitations.

DISCUSSION

Heterozygote $Tsc1^{+/-}$ mice develop renal cystadenomas, liver hemangiomas and, more rarely, extremity angiosarcomas, in a pattern that is very similar to that of $Tsc2^{+/-}$ mice (26,27). However, the extent of lesion development in the kidney is somewhat milder than that seen in $Tsc2^{+/-}$ mice, and $Tsc1^{-/-}$ embryos survive on average ~1 day longer than $Tsc2^{-/-}$ embryos. The basis for these differences is not evident, but could relate to some distinct function for tuberin, or be consistent with a more direct and critical function of tuberin in the tuberin–hamartin complex. Our pathologic and histologic findings are similar to those described recently in an independently derived Tsc1 null allele (31), although there are some differences in the two studies.

Kobayashi *et al.* (31) generated a Tsc1 null allele by deletion of exons 6–8 with insertion of a neo cassette. They demonstrated reduction of Tsc1 mRNA levels in null embryos but did not examine protein expression. Our deletion removes exons 17 and 18 of Tsc1, and we demonstrated an absence of hamartin expression in cultured $Tsc1^{-/-}$ MEFs, using a C-terminal antibody. Both deletions take the mRNA out of reading frame and, thus, are equivalent to naturally occurring TSC patient mutations in TSC1. There does not appear to be any difference in the phenotype of TSC based upon the site of mutation within TSC1, whereas there is a difference between TSC1 and TSC2 mutations (22). Kobayashi *et al.* (31) saw exencephaly in six of 19 embryos examined, whereas we saw it in none of 33 embryos ($P = 0.0006$), and brain development in our Tsc1 null embryos appeared normal. It is possible that the mutations generated have distinct consequences, but we suspect that strain differences, environmental factors or chance are more likely explanations. The overall milder phenotype of the Tsc1 null embryos (31; and our observations) fits well with the lack of this finding in our embryos. In addition, Kobayashi *et al.*

(31) did not find any premature mortality in female Tsc1$^{+/-}$ mice, a finding that was quite striking in our Tsc1$^{+/-}$ mice. We suspect that this is due to the prospective cohort approach that we took to evaluating morbidity and mortality in our colony. Strain differences may also contribute to this difference, as our data suggest that this pathologic development is particularly frequent in pure 129/SvJae.

Tsc1 null embryos die between E9.5 and E13.5 with prominent defects in liver development, coinciding with the timing of onset of hematopoeisis in the murine liver (32). Liver defects, as well as prominent cardiac enlargement, were seen by Kobayashi *et al.* (31) in their Tsc1 null embryos. Abnormalities of liver development correlate nicely with the major cause of mortality in the heterozygote mice, liver hemangioma formation. We demonstrate that these liver hemangiomas are more common, more extensive and cause greater mortality in female than in male Tsc1$^{+/-}$ mice (Fig. 3; Tables 2–4). These lesions share histologic features with both angiomyolipomas (AMLs), which occur in the kidney and liver in TSC patients, and LAM (1). Both AMLs and LAM are seen in TSC patients at relatively high frequency and also rarely occur in non-TSC patients. All three processes contain proliferating smooth muscle cells and both AMLs and mouse hemangiomas contain prominent disorganized blood vessels, which can bleed with fatal consequences. The predominance of these lesions in female mice suggests that female sex hormones influence their development, also similar to AMLs and LAM in TSC patients (2,33). Thus, these liver hemangiomas may serve as a model system for study of the pathogenesis of both of these important TSC tumors, including the role of female sex hormones and their receptors.

A biochemical function for either tuberin or hamartin has been elusive. Hamartin has been reported to bind to ezrin and other ERM family proteins and to interact with rho and the actin cytoskeleton in overexpression experiments (16). Using immortalized MEF lines we showed a difference in actin and focal adhesion dynamics in Tsc1 null compared to wild-type lines, supporting a function for hamartin in this system. The PI3kinase-PDK1-Akt signalling cascade and its many downstream branches has been identified as having important roles in many cellular activities including regulation of the actin cytoskeleton and motility, cellular and organismal glucose homeostasis, cell growth responses, apoptosis regulation and regulation of cell size (34–36). Recent screens carried out in *Drosophila* have identified a major role for the dTsc1 and dTsc2 genes in the control of cell size (28–30,37). Epistasis analysis has implicated these genes as acting downstream of dAkt and upstream of dS6K in some studies (29,30). However, the positioning of dTsc1 and dTsc2 relative to this pathway has been uncertain, and other studies have suggested that they may regulate nuclear events including cyclin levels (28,37). Moreover, the biochemical function of dTsc1 and dTsc2 relative to this pathway is unknown.

We demonstrate that both S6K and its substrate S6 are constitutively activated, as assessed by phosphorylation of each, in Tsc1 null MEFs. The 4E-BP1 protein is also hyperphosphorylated in these cells, consistent with activation of the mTOR protein (38). This activation of S6K and S6 is abolished by treatment of the Tsc1 null cells with rapamycin, a specific inhibitor of the mTOR protein (39). Therefore, these results suggest that hamartin, likely acting in the form of the tuberin–hamartin complex, influences mTOR directly or indirectly to diminish its activity in the phosphorylation and activation of S6K, and phosphorylation and inactivation of 4E-BP1 in normal cells. Absence of hamartin would lead to abrogation of this inhibition, with constitutive activation of mTOR and phosphorylation of its downstream partners S6K, S6 and 4E-BP1. The reduction in levels of pAkt in Tsc1 null cells following serum stimulation is also noteworthy. We suspect that this is due to some type of feedback inhibition of Akt activation caused by the constitutive activation of S6K in these cells.

Interestingly, patients with mutations in either PTEN, or TSC1 or TSC2, develop benign multicellular proliferations (hamartomas) (1,40). It is of interest that both of these proteins function within the PI3kinase-PDK1-Akt signalling pathway. The observation of increased amounts of p-S6 in tumors in the Tsc1 heterozygote mice suggests that activation of this pathway occurs in these tumors. Thus, treatment of these murine tumors with rapamycin or its analogues may have unique benefits that may be translatable to the care of TSC patients.

MATERIALS AND METHODS

Generation of a targeted Tsc1 allele in ES cells and mice

A murine Tsc1 genomic clone was isolated from a 129/Sv mouse BAC library. *Sac*I fragments (5 and 11 kb) containing Tsc1 exons 13–23 were cloned and sequenced. A gene targeting construct was made (Fig. 1A) and introduced into J1 ES cells as described previously (27,41). Forty clones were selected with 200 mg/l G418, minimally expanded and their DNA isolated and digested with *Bsa*BI, and analyzed by Southern blot using a flanking genomic probe (Fig. 1A). Two of seven ES clones that had undergone homologous recombination were electroporated with PICcre to express the cre recombinase, clones were isolated without selection and those undergoing deletion of Tsc1 exons were identified by Southern blotting and PCR analysis. Two of those deleted ES cell lines were then injected into blastocysts, followed by transfer to pseudopregnant female mice. Multiple chimeric offspring were obtained, and were bred with either wild-type C57BL/6J, BALB/cJ (Jackson Laboratories) or 129/SvJae mice to produce F1 animals.

Southern blot and PCR genotyping analyses of ES cells and mice

Tail snips were used to prepare DNA for Southern blot and PCR analysis from liveborn mice (41). Embryo or yolk sac fragments were used for analysis of embryos. PCR genotyping was performed by simultaneous amplification of both wild-type Tsc1 and the deleted allele using the following three primers in a 35 cycle PCR reaction using Perkin Elmer AmpliTaq Gold: F4536, 5′-AGGAGGCCTCTTCTGCTACC-3′; R4830, 5′-CAGCTCCGACCATGAAGTG-3′; and R6548, 5′-TGGGTCCTGACCTATCTCCTA-3′ (Fig. 1D). Products were 295 bp (wild-type) and 368 bp (mutant), and were analyzed on agarose gels.

Animal care, necropsy and pathology procedures

All procedures were carried out in accordance with the Guide for the Humane Use and Care of Laboratory Animals, and these studies were approved by the Harvard Medical Area Standing Committee on Animals. Embryonic age was determined by tracking vaginal plug formation and inspection of limb bud development. Embryo viability was determined by the presence of cardiac contractions. Three Tsc1 null embryos and three controls were serially sectioned in the sagital plane for histologic review.

Necropsy analysis included examination and sectioning of brain, heart, lungs, kidney and liver. Kidneys were cut into five dorso-ventral sections for histological examination. Standard H&E stains were used.

Immunohistochemistry and immunoblotting were performed on paraffin-embedded sections, and proteins separated by SDS–PAGE, respectively, as described previously (42). Protein was loaded at 20 µg per lane, except for the primary MEF cultures where only 10 µg was available. Immunoblots were developed with HRP-conjugated anti-rabbit antibodies using enhanced chemiluminescence (Pierce). Sections labelled with fluorescence were examined on a Nikon Diaphot 300 microscope with a Roper Instruments Micromax 1300y CCD. Images were acquired with an Innovision Image Processing System, and processed to achieve pseudo colors using Adobe Photoshop 5.0 software.

MEF culture and analysis

E10–10.5 embryos were collected from $Tsc1^{+/-}$ intercrosses. Embryos were triturated in DMEM, and then plated in DMEM with 10% fetal calf serum in 5% CO_2. Cells were passaged and replated at constant density (1.5×10^4 per cm^2) every 3–4 days. Serum deprivation for 1–2 days and restimulation for 30–60 min was performed under conditions of constant temperature. Cell lysates were prepared by scraping to collect cells on ice, followed by addition of extraction buffer containing 2% SDS, 0.1 M DTT, 60 mM Tris–HCl pH 6.8, 10% glycerol, followed by immediate boiling. LY294002 and rapamycin were obtained from Cell Signalling Technology, and used at 10 µM and 10 nM, respectively.

Antibodies against hamartin were prepared in rabbits by injection of a bacterially expressed 6×His-tagged protein fragment encoding the C-terminal 204 amino acids of human hamartin. Anti-murine gelsolin antibody was prepared previously (43). Other antibodies were obtained from: tuberin (Santa Cruz C-20); Cy3 labelled monoclonal anti-smooth muscle actin (Sigma); p-Akt (Ser473), Akt, p-S6K (Thr389), S6K, p-S6 (Ser235/236, Ser240/244), S6 and p-4E-BP1 (Thr37) (all from Cell Signalling Technology); monoclonal paxillin (ICN Biomedical). Secondary antibodies were rhodamine-labelled donkey anti-mouse and fluorescein-conjugated donkey anti-rabbit (Jackson Immunochemical).

For analysis of focal adhesions and actin stress fibres, cells were grown on glass coverslips and, after treatments, were fixed with 3.7% paraformaldehyde and permeabilized with 0.1% Triton X-100. Focal adhesions were labelled with the anti-paxillin antibody and F-actin was labelled with FITC–phalloidin (Sigma). Staining intensity of stress fibres and focal adhesions were quantified using NIH Image to measure the average pixel intensity per cell.

Statistics

Kaplan–Meier cumulative survival plots were calculated using Statview v5.0 and comparisons made using the logrank (Mantel–Cox) test. The average number of tumours per mouse was compared using the two-sample *t*-test, and when mixed by sex and strain, using analysis of covariance. The SAS statistical package was applied by Tim Heeren (Boston University School of Public Health).

ACKNOWLEDGEMENTS

We thank Richard Lamb, William Sellers and Chris Carpenter for helpful discussions, Arlene Sharpe for the use of the BWH Transgenic Core Facility, Rod Bronson for assistance with mouse pathology, Penelope Roberts for technical assistance, and William Watts for support. This work was supported by the NIH NINDS, grants NS31535 and NS41498, the Tuberous Sclerosis Alliance and the March of Dimes.

REFERENCES

1. Gomez,M., Sampson,J. and Whittemore,V. (1999) *The Tuberous Sclerosis Complex*. Oxford University Press, Oxford, UK.
2. Johnson,S.R. and Tattersfield,A.E. (2000) Clinical experience of lymphangioleiomyomatosis in the UK. *Thorax*, **55**, 1052–1057.
3. Franz,D.N., Brody,A., Meyer,C., Leonard,J., Chuck,G., Dabora,S., Sethuraman,G., Colby,T.V., Kwiatkowski,D.J. and McCormack,F.X. (2001) Mutational and radiographic analysis of pulmonary disease consistent with lymphangioleiomyomatosis and micronodular pneumocyte hyperplasia in women with tuberous sclerosis. *Am. J. Respir. Crit. Care Med.*, **164**, 661–668.
4. Au,K.S., Hebert,A.A., Roach,E.S. and Northrup,H. (1999) Complete inactivation of the TSC2 gene leads to formation of hamartomas. *Am. J. Hum. Genet.*, **65**, 1790–1795.
5. Henske,E.P., Scheithauer,B.W., Short,M.P., Wollmann,R., Nahmias,J., Hornigold,N., van Slegtenhorst,M., Welsh,C.T. and Kwiatkowski,D.J. (1996) Allelic loss is frequent in tuberous sclerosis kidney lesions but rare in brain lesions. *Am. J. Hum. Genet.*, **59**, 400–406.
6. Carbonara,C., Longa,L., Grosso,E., Mazzucco,G., Borrone,C., Garre,M.L., Brisigotti,M., Filippi,G., Scabar,A., Giannotti,A. *et al.* (1996) Apparent preferential loss of heterozygosity at TSC2 over TSC1 chromosomal region in tuberous sclerosis hamartomas. *Genes Chromosomes Cancer*, **15**, 18–25.
7. Green,A.J., Smith,M. and Yates,J.R. (1994) Loss of heterozygosity on chromosome 16p13.3 in hamartomas from tuberous sclerosis patients. *Nat. Genet.*, **6**, 193–196.
8. Niida,Y., Stemmer-Rachamimov,A.O., Logrip,M., Tapon,D., Perez,R., Kwiatkowski,D.J., Sims,K., MacCollin,M., Louis,D.N. and Ramesh,V. (2001) Survey of somatic mutations in tuberous sclerosis complex (TSC) hamartomas suggests different genetic mechanisms for pathogenesis of TSC lesions. *Am. J. Hum. Genet.*, **69**, 493–503.
9. The European Tuberous Sclerosis Consortium (1993) Identification and characterization of the tuberous sclerosis gene on chromosome 16. *Cell*, **75**, 1305–1315.
10. van Slegtenhorst,M., de Hoogt,R., Hermans,C., Nellist,M., Janssen,B., Verhoef,S., Lindhout,D., van den Ouweland,A., Halley,D., Young,J. *et al.* (1997) Identification of the tuberous sclerosis gene TSC1 on chromosome 9q34. *Science*, **277**, 805–808.
11. Xiao,G.H., Shoarinejad,F., Jin,F., Golemis,E.A. and Yeung,R.S. (1997) The tuberous sclerosis 2 gene product, tuberin, functions as a Rab5 GTPase activating protein (GAP) in modulating endocytosis. *J. Biol. Chem.*, **272**, 6097–6100.
12. Wienecke,R., Konig,A. and DeClue,J.E. (1995) Identification of tuberin, the tuberous sclerosis-2 product. Tuberin possesses specific Rap1GAP activity. *J. Biol. Chem.*, **270**, 16409–16414.
13. Tsuchiya,H., Orimoto,K., Kobayashi,K. and Hino,O. (1996) Presence of potent transcriptional activation domains in the predisposing tuberous sclerosis (Tsc2) gene product of the Eker rat model. *Cancer Res.*, **56**, 429–433.

14. Soucek,T., Yeung,R.S. and Hengstschlager,M. (1998) Inactivation of the cyclin-dependent kinase inhibitor p27 upon loss of the tuberous sclerosis complex gene-2. *Proc. Natl Acad. Sci. USA*, **95**, 15653–15658.
15. Henry,K.W., Yuan,X., Koszewski,N.J., Onda,H., Kwiatkowski,D.J. and Noonan,D.J. (1998) Tuberous sclerosis gene 2 product modulates transcription mediated by steroid hormone receptor family members. *J. Biol. Chem.*, **273**, 20535–20539.
16. Lamb,R.F., Roy,C., Diefenbach,T.J., Vinters,H.V., Johnson,M.W., Jay,D.G. and Hall,A. (2000) The TSC1 tumour suppressor hamartin regulates cell adhesion through ERM proteins and the GTPase Rho. *Nat. Cell Biol.*, **2**, 281–287.
17. van Slegtenhorst,M., Nellist,M., Nagelkerken,B., Cheadle,J., Snell,R., van den Ouweland,A., Reuser,A., Sampson,J., Halley,D. and van der Sluijs,P. (1998) Interaction between hamartin and tuberin, the TSC1 and TSC2 gene products. *Hum. Mol. Genet.*, **7**, 1053–1058.
18. Plank,T.L., Yeung,R.S. and Henske,E.P. (1998) Hamartin, the product of the tuberous sclerosis 1 (TSC1) gene, interacts with tuberin and appears to be localized to cytoplasmic vesicles. *Cancer Res.*, **58**, 4766–4770.
19. Sampson,J.R., Scahill,S.J., Stephenson,J.B., Mann,L. and Connor,J.M. (1989) Genetic aspects of tuberous sclerosis in the west of Scotland. *J. Med. Genet.*, **26**, 28–31.
20. Jones,A.C., Shyamsundar,M.M., Thomas,M.W., Maynard,J., Idziaszczyk,S., Tomkins,S., Sampson,J.R. and Cheadle,J.P. (1999) Comprehensive mutation analysis of TSC1 and TSC2 and phenotypic correlations in 150 families with tuberous sclerosis. *Am. J. Hum. Genet.*, **64**, 1305–1315.
21. Cheadle,J.P., Reeve,M.P., Sampson,J.R. and Kwiatkowski,D.J. (2000) Molecular genetic advances in tuberous sclerosis. *Hum. Genet.*, **107**, 97–114.
22. Dabora,S.L., Jozwiak,S., Franz,D.N., Roberts,P.S., Nieto,A., Chung,J., Choy,Y.S., Reeve,M.P., Thiele,E., Egelhoff,J.C. *et al.* (2001) Mutational analysis in a cohort of 224 tuberous sclerosis patients indicates increased severity of TSC2, compared with TSC1, disease in multiple organs. *Am. J. Hum. Genet.*, **68**, 64–80.
23. Eker,R., Mossige,J., Johannessen,J.V. and Aars,H. (1981) Hereditary renal adenomas and adenocarcinomas in rats. *Diagn. Histopath.*, **4**, 99–110.
24. Yeung,R.S., Xiao,G.H., Jin,F., Lee,W.C., Testa,J.R. and Knudson,A.G. (1994) Predisposition to renal carcinoma in the Eker rat is determined by germ-line mutation of the tuberous sclerosis 2 (TSC2) gene. *Proc. Natl Acad. Sci. USA*, **91**, 11413–11416.
25. Kobayashi,T., Hirayama,Y., Kobayashi,E., Kubo,Y. and Hino,O. (1995) A germline insertion in the tuberous sclerosis (Tsc2) gene gives rise to the Eker rat model of dominantly inherited cancer. *Nat. Genet.*, **9**, 70–74.
26. Kobayashi,T., Minowa,O., Kuno,J., Mitani,H., Hino,O. and Noda,T. (1999) Renal carcinogenesis, hepatic hemangiomatosis, and embryonic lethality caused by a germ-line Tsc2 mutation in mice. *Cancer Res.*, **59**, 1206–1211.
27. Onda,H., Lueck,A., Marks,P.W., Warren,H.B. and Kwiatkowski,D.J. (1999) Tsc2(+/–) mice develop tumors in multiple sites that express gelsolin and are influenced by genetic background. *J. Clin. Invest.*, **104**, 687–695.
28. Tapon,N., Ito,N., Dickson,B.J., Treisman,J.E. and Hariharan,I.K. (2001) The *Drosophila* tuberous sclerosis complex gene homologs restrict cell growth and cell proliferation. *Cell*, **105**, 345–355.
29. Potter,C.J., Huang,H. and Xu,T. (2001) *Drosophila* tsc1 functions with tsc2 to antagonize insulin signaling in regulating cell growth, cell proliferation, and organ size. *Cell*, **105**, 357–368.
30. Gao,X. and Pan,D. (2001) TSC1 and TSC2 tumor suppressors antagonize insulin signaling in cell growth. *Genes Dev.*, **15**, 1383–1392.
31. Kobayashi,T., Minowa,O., Sugitani,Y., Takai,S., Mitani,H., Kobayashi,E., Noda,T. and Hino,O. (2001) A germ-line Tsc1 mutation causes tumor development and embryonic lethality that are similar, but not identical to, those caused by Tsc2 mutation in mice. *Proc. Natl Acad. Sci. USA*, **98**, 8762–8767.
32. Muller,A.M., Medvinsky,A., Strouboulis,J., Grosveld,F. and Dzierzak,E. (1994) Development of hematopoietic stem cell activity in the mouse embryo. *Immunity*, **1**, 291–301.
33. van Baal,J.G., Smits,N.J., Keeman,J.N., Lindhout,D. and Verhoef,S. (1994) The evolution of renal angiomyolipomas in patients with tuberous sclerosis. *J. Urol.*, **152**, 35–38.
34. Belham,C., Comb,M.J. and Avruch,J. (2001) Identification of the NIMA family kinases NEK6/7 as regulators of the p70 ribosomal S6 kinase. *Curr. Biol.*, **11**, 1155–1167.
35. Blume-Jensen,P. and Hunter,T. (2001) Oncogenic kinase signalling. *Nature*, **411**, 355–365.
36. Gingras,A.C., Raught,B. and Sonenberg,N. (2001) Regulation of translation initiation by FRAP/mTOR. *Genes Dev.*, **15**, 807–826.
37. Ito,N. and Rubin,G.M. (1999) gigas, a *Drosophila* homolog of tuberous sclerosis gene product-2, regulates the cell cycle. *Cell*, **96**, 529–539.
38. Gingras,A.C., Gygi,S.P., Raught,B., Polakiewicz,R.D., Abraham,R.T., Hoekstra,M.F., Aebersold,R. and Sonenberg,N. (1999) Regulation of 4E-BP1 phosphorylation: a novel two-step mechanism. *Genes Dev.*, **13**, 1422–1437.
39. Sabers,C.J., Martin,M.M., Brunn,G.J., Williams,J.M., Dumont,F.J., Wiederrecht,G. and Abraham,R.T. (1995) Isolation of a protein target of the FKBP12-rapamycin complex in mammalian cells. *J. Biol. Chem.*, **270**, 815–822.
40. Eng,C. (1998) Genetics of Cowden syndrome: through the looking glass of oncology. *Int. J. Oncol.*, **12**, 701–710.
41. Witke,W., Sharpe,A.H., Hartwig,J.H., Azuma,T., Stossel,T.P. and Kwiatkowski,D.J. (1995) Hemostatic, inflammatory, and fibroblast responses are blunted in mice lacking gelsolin. *Cell*, **81**, 41–51.
42. Lueck,A., Brown,D. and Kwiatkowski,D. (1998) The actin-binding proteins adseverin and gelsolin are both highly expressed but differentially localized in kidney and intestine. *J. Cell Sci.*, **111**, 3633–3643.
43. Azuma,T., Witke,W., Stossel,T.P., Hartwig,J.H. and Kwiatkowski,D.J. (1998) Gelsolin is a downstream effector of rac for fibroblast motility. *EMBO J.*, **17**, 1362–1370.